UC Riverside
UC Riverside Previously Published Works

Title
Modeling the release of E. coli D21g with transients in water content

Permalink
https://escholarship.org/uc/item/6bk632fx

Journal
Water Resources Research, 51(5)

ISSN
0043-1397

Authors
Bradford, Scott A
Wang, Yusong
Torkzaban, Saeed
et al.

Publication Date
2015-05-01

DOI
10.1002/2014wr016566

Peer reviewed

RESEARCH ARTICLE

Key Points:
- A model of colloid release with transients in water saturation
- The model provided a good description of published data
- Numerical experiments were performed to understand factors controlling release

Correspondence to:
S. A. Bradford,
Scott.Bradford@ars.usda.gov

Modeling the release of *E. coli* D21g with transients in water content

Scott A. Bradford[1], Yusong Wang[2], Saeed Torkzaban[3], and Jiri Šimůnek[2]

[1]US Salinity Laboratory, USDA, ARS, Riverside, California, USA, [2]Department of Environmental Sciences, University of California, Riverside, California, USA, [3]CSIRO Land and Water, Glen Osmond, South Australia, Australia

Abstract Transients in water content are well known to mobilize colloids that are retained in the vadose zone. However, there is no consensus on the proper model formulation to simulate colloid release during drainage and imbibition. We present a model that relates colloid release to changes in the air-water interfacial area (A_{aw}) with transients in water content. Colloid release from the solid-water interface (SWI) is modeled in two steps. First, a fraction of the colloids on the SWI partitions to the mobile aqueous phase and air-water interface (AWI) when the A_{aw} increases during drainage. Second, colloids that are retained on the AWI or at the air-water-solid triple line are released during imbibition as the AWI is destroyed. The developed model was used to describe the release of *Escherichia coli* D21g during cycles of drainage and imbibition under various saturation conditions. Simulations provided a reasonable description of experimental D21g release results. Only two model parameters were optimized to the D21g release data: (i) the cell fraction that was released from the SWI (f_r) and (ii) the cell fraction that partitioned from the SWI to the AWI (f_{awi}). Numerical simulations indicated that cell release was proportional to f_r and the initial amount of retention on the SWI and AWI. Drainage to a lower water content enhanced cell release, especially during subsequent imbibition, because more bacteria on the SWI were partitioned to the AWI and/or aqueous phase. Imbibition to a larger water content produced greater colloid release because of higher flow rates, and more destruction of the AWI (smaller A_{aw}). Variation in the value of f_{awi} was found to have a pronounced influence on the amount of cell release in both drainage and imbibition due to changes in the partitioning of cells from the SWI to the aqueous phase and the AWI.

1. Introduction

Transients in water content commonly occur in the vadose zone as a result of infiltration and redistribution, evapotranspiration, and fluctuations in the water table height and/or surface water levels (waves, tides, and river stage). Considerable amounts of research have demonstrated that retained colloids in soils can be remobilized by sudden changes in water content [*Saiers et al.*, 2003; *Saiers and Lenhart*, 2003; *Auset et al.*, 2005; *Gao et al.*, 2006; *Zhuang et al.*, 2007; *Shang et al.*, 2008; *Cheng and Saiers*, 2009; *Engstrom et al.*, 2015]. Released colloids may be contaminants of concern such as pathogenic microorganisms [*Zhang et al.*, 2012; *Russell et al.*, 2012] or nanoparticles [*Chen et al.*, 2008], or can facilitate the transport of many adsorbed contaminants [*Cheng and Saiers*, 2010]. Consequently, an understanding and ability to predict the release of colloids with transients in water content are needed to protect water resources and human health.

Column-scale studies have been conducted to investigate colloid retention and release during unsaturated conditions [*Cherrey et al.*, 2003; *Gao et al.*, 2004; *Chen and Flury*, 2005; *Cheng and Saiers*, 2009; *Shang et al.*, 2008; *Zhuang et al.*, 2007, 2009]. Colloid retention has commonly been reported to increase with a decrease in water content under steady state unsaturated flow conditions [*Wan and Wilson*, 1994; *Schafer et al.*, 1998; *Gargiulo et al.*, 2008; *Torkzaban et al.*, 2006a, b, 2008]. Conversely, a diversity of results has been reported for colloid release during transients in water saturation, and there is no concensus on the relative importance of drainage and imbibition. Some studies have attributed colloid release only to imbibition [*Russell et al.*, 2012], whereas others have observed colloid release during both drainage and imbibition [*Zhuang et al.*, 2009; *Cheng and Saiers*, 2009; *Zhang et al.*, 2012]. Greater colloid release has commonly been observed during imbibition [*Saiers and Lenhart*, 2003; *Auset et al.*, 2005; *Gao et al.*, 2006; *Zhuang et al.*, 2007], but drainage has also been reported to produce greater colloid release [*Cheng and Saiers*, 2009]. These discrepancies are

likely due to differences in the initial conditions, the saturation dynamics, and variations in colloid and soil properties (hydrophobicity, size, and shape) and solution chemistry [*Aramrak et al.*, 2014; *Wang et al.*, 2014].

Pore-scale studies have been conducted to better understand mechanisms influencing the release of colloids during drainage and imbibition [*Gómez-Suárez et al.*, 2001; *Gao et al.*, 2006; *Lazouskaya and Jin*, 2008, *Lazouskaya et al.*, 2011, 2013; *Sharma et al.*, 2008; *Zevi et al.*, 2012; *Aramrak et al.*, 2013]. In water-wet porous media, air invades the soil pore spaces during water drainage starting from the larger pores then to successively smaller regions of the pore space. The air-water interfacial area (A_{aw}) increases as receding water films cover drained portions of the solid-water interface (SWI). These water films are thin, with reported thickness ranging from a few nm up to 100 nm [*Wan and Tokunaga*, 1997; *Shang et al.*, 2009; *Chatterjee et al.*, 2012; *Lazouskaya et al.*, 2013]. In addition to electrostatic and van der Waals interactions from the SWI and air-water interface (AWI), a strong capillary force will act on retained colloids on the SWI if the water film thickness (w_f) is smaller than the colloid diameter (d_c) [*Schafer et al.*, 1998; *Saiers and Lenhart*, 2003; *Lazouskaya et al.*, 2011]. Consequently, colloids that are retained on the SWI experience different forces and torques as w_f decreases during drainage [*Lazouskaya et al.*, 2013]. The colloids will begin to experience interaction energies arising from both the SWI and AWI as w_f decreases, which will alter the force and torque balance at a particular location, and may mobilize some of the colloids from the SWI to the aqueous phase or partition colloids from the SWI to the AWI [*Wang et al.*, 2014].

Destruction of the AWI occurs as the air-water-solid (AWS) contact line advances from smaller to larger pore spaces during water imbibition. This process produces a decrease in A_{aw}, expansion of water films, and elimination of AWS triple lines that may result in mobilization of colloids from the AWI to the aqueous phase [*Auset et al.*, 2005; *Gao et al.*, 2006; *Chen et al.*, 2008; *Cheng and Saiers*, 2009]. Results demonstrate that colloid release is typically much more efficient during imbibition than drainage [*Lazouskaya et al.*, 2008, 2011; *Aramrak et al.*, 2011; *Wang et al.*, 2014]. The amount of colloid release during imbibition has been reported to depend on the colloid size and shape [*Gómez-Suárez et al.*, 2001; *Aramrak et al.*, 2013], the water film thickness [*Wan and Tokunaga*, 1997], the surface tension [*Gómez-Suárez et al.*, 2001], the velocity of the advancing AWI [*Saiers and Lenhart*, 2003], and the hydrophobicity of the solid surface and colloid [*Lazouskaya et al.*, 2013].

The above information strongly indicates that the AWS triple line and A_{aw} play critical roles in colloid release during transient water content conditions. Conversely, existing mathematical models that simulate colloid release during drainage and imbibition do not explicitly consider all relevant exchange process and interfaces. For example, the models of *Saiers and Lenhart* [2003], *Cheng and Saiers* [2009], and *Russell et al.* [2012] only consider release of colloids from the SWI to the aqueous phase. In this case, the kinetic release rate is assumed to be proportional to the pore water velocity [*Saiers and Lenhart*, 2003] or temporal changes in the water content during imbibition [*Russell et al.*, 2012] or drainage and imbibition [*Cheng and Saiers*, 2009]. However, these models did not consider colloid release from the SWI to the AWI, accumulation of colloids on the AWI, or release of colloids from the AWI to the aqueous phase. *Zhang et al.* [2012] employed a linear equilibrium model to account for virus interactions at the AWI. The retardation coefficient was a function A_{aw} that increased as the water content decreased. However, this model did not explicitly consider colloid release from the SWI to the AWI.

The objective of this research is to improve our ability to predict colloid release with transients in water saturation. In particular, we have developed a model that explicitly considers colloid release from the SWI to the aqueous phase and the AWI, colloid accumulation at the AWI, and colloid release from the AWI to the aqueous phase as a result of temporal changes in the A_{aw} during transient water content conditions. The developed model was subsequently used to simulate colloid release data from *Wang et al.* [2014] over a wide range of water saturation conditions. Results provide valuable insight on the effects of water saturation dynamics on colloid release.

2. Experimental Information

Wang et al. [2014] presented breakthrough and release curves for *Escherichia coli* D21g under transient water saturation conditions. Experimental details are given in this publication, but will be briefly highlighted below. Ottawa sand that is 120 μm in size was cleaned using a salt cleaning method [*Bradford and Kim*, 2010] to remove trace amounts of clay. A 5 mM NaCl solution at pH = 5.8 was prepared for the resident,

Table 1. Summary of Experimental Conditions for Breakthrough (Phases 1 and 2) and Release (Phase 3) Experiments[a]

Figure #	Phase	Cell Suspension PVs	Cycle	Step	Ending Saturation	Top Flux (mL/min)	Bottom Pressure (cm)
2	1, 2	2.2			0.64	6.5	−90
2	3		1	I1	0.71	21.3	−90
2	3		1	I2	0.82	39.1	−90
3	1, 2	1.6			1	45.6	0
3	3		1	D1	0.36	0	−90
3	3		1	I1	0.71	24.3	−90
4a	1, 2	3.1			1	42.6	0
4a	3		1	D1	0.34	0	−90
4a	3		1	I1	0.71	23.5	−90
4a	3		1	I2	0.83	41.2	−90
4a	3		2	D2	0.35	0	−90
4a	3		2	I3	0.71	23.5	−90
4a	3		2	I4	0.82	41.2	−90
4a	3		3	D3	0.34	0	−90
4a	3		3	I5	0.69	23.5	−90
4a	3		3	I6	0.80	41.2	−90
4a	3		4	D4	0.35	0	−90
4a	3		4	I7	0.71	23.5	−90
4a	3		4	I8	0.82	41.2	−90
4b	1, 2	1.6			1	42.7	0
4b	3		1	D1	0.57	0	−90
4b	3		1	I1	0.83	42.7	−90
4b	3		2	D2	0.36	0	−90
4b	3		2	I2	0.86	42.7	−90
4b	3		3	D3	0.27	0	−100
4b	3		3	I3	0.86	42.7	−100

[a]D# denotes drainage number (#); I# denotes imbibition number (#).

tracer, and eluting solutions during the transport experiments. The influent cell concentration (C_o) was equal to approximately 10^8 cells mL^{-1}. Zeta potentials of the sand and cells, and the corresponding interaction energy for this solution chemistry were calculated.

The sand was wet packed into a 13.2 cm diameter by 22 cm long column to a height of 20 cm. The porosity (ε) of the packed column was about 0.34. Several pore volumes (PVs) of 5 mM NaCl solution were pumped to the top of the column at a steady Darcy velocity to allow the sand to equilibrate with the solution. A step pulse of *E. coli* D21g suspension was then injected at the top of the column (Phase 1) followed by continued flushing with the cell-free eluting solution at the same velocity and solution chemistry (Phase 2). Saturated conditions were maintained in the column by keeping a small layer of ponding at the column top and a zero pressure head at the bottom boundary. Steady state water flow conditions at a selected water saturation were achieved by reducing the inflow rate at the column top and increasing the suction at the bottom boundary with a hanging water column until a unit hydraulic head gradient was obtained (the column was equipped with tip tensiometers at depths of 5, 10, and 15 cm from the column top to measure the hydraulic head).

Phase 3 consisted of various drainage and/or imbibition conditions to study the release of D21g. Drainage was conducted with no flow at the column top while maintaining a negative pressure at the bottom of the column. Imbibition was initiated by increasing the flow rate at the column top and/or increasing the bottom boundary pressure. Cell concentrations in the column effluent (Phases 1–3) were monitored over time with a spectrophotometer. The total water saturation in the column was continuously monitored with an electronic balance.

Table 1 provides a summary of experimental conditions for D21g breakthrough (Phases 1 and 2) and release (Phase 3) experiments.

3. Mathematical Model

3.1. Water Flow
Variably saturated water flow is described using Richards' equation [*Richards*, 1931] in the vertical direction as

Table 2. Fitted Parameter Values for the Unsaturated Soil Hydraulic Property Model of *van Genuchten* [1980], and the Pearson's Correlation Coefficient (R^2)[a]

Figure #	θ_r	θ_s	α (cm^{-1})	n	l	K_s (cm min^{-1})	R^2
2	0.03	0.34	0.012	2.69	0.00	0.30	1.00
3	0.00	0.34	0.016	3.25	0.66	0.23	1.00
4a	0.03	0.36	0.013	5.07	0.00	0.31	1.00
4b	0.00	0.34	0.016	3.25	0.66	0.23	1.00

[a]θ_r denotes the residual water content, θ_s denotes the saturated water content, α denotes the reciprocal of the air entry pressure, n denotes the pore size distribution parameter, with $m = 1 - 1/n$, l denotes the pore-connectivity parameter, and K_s denotes the saturated hydraulic conductivity.

$$\frac{\partial \theta}{\partial t} = \frac{\partial}{\partial z}\left(K(\theta)\frac{\partial h}{\partial z}\right) - \frac{\partial K(\theta)}{\partial z},$$ (1)

where z [L; L denotes units of length] is the distance in the vertical direction, t [T; T denotes unit of time] is the time, θ [L^{3}L^{-3}] is the volumetric water content, K [LT^{-1}] is the unsaturated hydraulic conductivity, and h [L] is the pressure head. The parameters for the unsaturated soil hydraulic properties were obtained by inverse optimization to experimental outflow information. Note that these parameters were constant during subsequent transport and release simulations. Table 2 provides a summary of the soil hydraulic property parameters, along with the Pearson's correlation coefficient (R^2). The value of R^2 was always greater than 0.99. This agreement indicates that the water contents and pore water velocities in the column were accurately captured by the model.

3.2. Colloid Transport in the Aqueous Phase
Colloid transport in the aqueous phase is described using the advective dispersion equation that includes terms for exchange to/from the SWI and AWI

$$\frac{\partial \theta_w C}{\partial t} = \frac{\partial}{\partial z}\left(\theta_w D\frac{\partial C}{\partial z}\right) - \frac{\partial q_w C}{\partial z} - E_{sw} - E_{aw},$$ (2)

where C [NL^{-3}; N denotes number] is the colloid concentration in the aqueous phase, D [L^{2}T^{-1}] is the hydrodynamic dispersion coefficient for colloids, q_w [LT^{-1}] is the Darcy water velocity, E_{sw} [NL^{-3}T^{-1}] is the exchange term between the aqueous phase and the SWI, E_{aw} [NL^{-3}T^{-1}] is the exchange terms between the aqueous phase and the AWI, and θ_w [L^{3}L^{-3}] is the volumetric water content that is accessible to colloids. The first and second terms on the right-hand side of equation (2) account for the dispersive and advective fluxes of the colloids, respectively. The dispersivity (D/v; where v [LT^{-1}] is the pore water velocity) was set equal to 0.1 cm based on published tracer results [*Wang et al.*, 2013]. It should be mentioned that θ_w is assumed to be equal to θ in this work. However, it is possible that θ_w may sometime be less than θ because of size and/or ion exclusion. *Šimůnek et al.* [2006] discusses the determination of θ_w for this situation.

3.3. Colloids at the Solid-Water Interface
The solid phase mass balance equation for colloids and E_{sw} (equation (2)) are given as

$$\rho_b \frac{\partial S}{\partial t} = \theta_w \psi_{sw} k_{sw} C - \rho_b k_{rs} S - E_{swa},$$ (3)

$$E_{sw} = \theta_w \psi_{sw} k_{sw} C - \rho_b k_{rs} S - (1 - f_{awi}) E_{swa},$$ (4)

where S [N M^{-1}; M denotes unit of mass] is the solid phase colloid concentration, ρ_b [M L^{-3}] is the bulk density, k_{sw} [T^{-1}] is the retention rate coefficient to the SWI, k_{rs} [T^{-1}] is the steady state release rate coefficient from the SWI, ψ_{sw} is a dimensionless blocking function on the SWI, E_{swa} [NL^{-3}T^{-1}] is the colloid exchange term from the SWI due to water drainage, and f_{awi} is the fraction of colloids released from the SWI that partitions to the AWI. Note that the right sides of equations (3) and (4) are not equal because only a fraction of E_{swa} partitions to the aqueous phase (e.g., $1 - f_{awi}$). As discussed below, the complementary fraction of E_{swa} partitions to the AWI (defined by f_{awi}).

The first and second terms on the right-hand side of equations (3) and (4) account for colloid retention and diffusive release, respectively, during Phases 1 and 2. The Langmuir model assumes that ψ_{sw} is a linear function of S that is given as [*Adamczyk et al.*, 1994]

Table 3. Summary of Mass Balance Information, Model Parameters, and Pearson's Correlation Coefficient for Observed and Simulated Breakthrough Curves (Phases 1 and 2)

Figure #	IS (mM)	Mass Recovery (%)	k_{sw} (min^{-1})	k_{rs} (min^{-1})	S_{max}/C_o (cm^3 g^{-1})	k_{aw} (min^{-1})	R^2
2[a]	5	19.3	0.027	0.001	0.606	0.0025	0.98
3	5	38.5	0.079	0.002	0.328		0.98
4a	5	33.2	0.089	0.003	0.810		0.92
4b	5	38.2	0.080	0.003	0.280		0.98

[a]Water saturation was 0.64.

$$\psi_{sw} = 1 - \frac{S}{S_{\max}}, \tag{5}$$

where S_{max} [NM^{-1}] is the maximum colloid concentration on the SWI. The parameters k_{sw}, k_{rs}, and S_{max} were obtained by inverse optimization to breakthrough curve (BTC) data under steady state flow and constant saturation conditions (Table 3). This information determines the initial colloid concentration on the SWI as a function of distance for subsequent release during Phase 3. Values of k_{sw} and k_{rs} were set to zero during Phase 3 because their functional dependency on θ_w was unknown, and it was not possible to experimentally quantify the simultaneous retention and release separately. Consequently, E_{swa} reflects the net effects of retention and release on the SWI during Phase 3, but it was equal to zero during Phases 1 and 2.

3.4. Colloids at the Air-Water Interface
In addition to the SWI, colloid retention and release may also occur on the AWI under unsaturated conditions. The mass balance equation for colloids at the AWI and E_{aw} (equation (2)) may be described as

$$\frac{\partial A_{aw}\Gamma}{\partial t} = \theta_w k_{aw} C + f_{awi} E_{swa} - E_{ra}, \tag{6}$$

$$E_{aw} = \theta_w k_{aw} C - E_{ra}, \tag{7}$$

where A_{aw} [L^{2}L^{-3}] is the total air-water interfacial area per unit volume, Γ [NL^{-2}] is the colloid concentration retained on the AWI, k_{aw} [T^{-1}] is the retention rate coefficient on the AWI, and E_{ra} [NL^{-3}T^{-1}] is the exchange term for colloids on the AWI to the aqueous phase due to destruction of the AWI during imbibition. Note that the right sides of equations (6) and (7) are not equal because only a fraction of E_{swa} partitions to the AWI.

The value of A_{aw} in equations (6) and (7) accounts for the area of interfaces between bulk fluids (e.g., the specific interfacial area) and the area of wetting films in drained portions of the pore space. It may be quantified as [*Bradford and Leij*, 1997] as

$$A_{aw}(\theta) = \frac{1}{\sigma_{aw}} \int_{\theta}^{\theta_s} P_{aw}(\theta) d\theta, \tag{8}$$

where σ_{aw} [M T^{-2}] is the air-water surface tension, P_{aw} [M L^{-1} T^{-2}] is the capillary pressure, and θ_s is the saturated water content. Consequently, information about the capillary pressure-saturation curve for a porous media can be used to determine $A_{aw}(\theta)$. Figure 1 shows a representative plot of A_{aw} as a function of θ for the sand employed in the study of *Wang et al.* [2014]. The value of A_{aw} increases with a decrease in θ and approaches the geometric surface area of the porous media (A_s, L^{2}L^{-3}) as θ goes to 0 [*Leverett*, 1941]. Note that equation (8) indicates that $\frac{dA_{aw}}{d\theta}$ is equal to $-\frac{P_{aw}(\theta)}{\sigma_{aw}}$.

The first term on right-hand side of equations (6) and (7) accounts for colloid retention to the AWI during Phases 1 and 2. The value of k_{aw} is expected to be a linear function of A_{aw} that is accessible to colloids in the aqueous phase [*Kim et al.*, 2008]. Diffusive detachment was assumed to be negligible because strong capillary forces act on colloids at the AWI [*Schafer et al.*, 1998]. Blocking was also neglected because it was not possible to uniquely determine its effects on both the SWI and AWI, and the observed blocking behavior in *Wang et al.* [2014] was similar under saturated and unsaturated conditions.

Experimental mass balance information was used to constrain the optimization of SWI (k_{sw}, k_{rs}, and S_{max}) and AWI (k_{aw}) retention parameters to the BTC under steady state, unsaturated conditions (Table 3). In particular, the amount of retention on the AWI was estimated as the difference in colloid retention in saturated
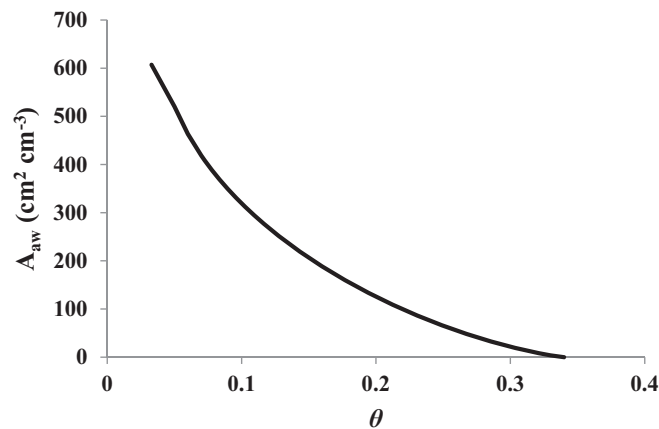
Figure 1. A representative plot of the air-water interfacial area (A_{aw}) as a function of water content (θ) for the sand employed by *Wang et al.* [2014]. The value of A_{aw} was calculated using equation (8).

and unsaturated conditions. Note that we do not attempt to differentiate various mechanisms of colloid retention in unsaturated systems (e.g., film straining, attachment to the AWI, and retention at the AWS triple line). Rather, this information was used to determine the initial colloid concentration that was associated with the SWI and AWI as a function of distance for subsequent release during Phase 3. The value of k_{aw} was set to zero during Phase 3 for similar reasons as k_{sw} and k_{rs} that are discussed above. Consequently, E_{swa} and E_{ra} reflect the net effects of retention and release on the SWI and AWI, respectively, during Phase 3, but they were equal to zero during Phases 1 and 2.

3.5. Transient Exchange Terms

The above model indicates that values of E_{swa} (equations (3), (4), and (6)) and E_{ra} (equations (6) and (7)) need to be determined in order to simulate the release of colloids during transient water content conditions. Each of these issues will be discussed below.

The amount of colloids that will remain solely on the SWI after drainage is given as

$$S = S_i F_{ND}(\theta) + S_i(1-f_r)(1-F_{ND}(\theta)). \tag{9}$$

Here S_i [N M^{-1}] is the initial solid phase concentration of retained colloids before drainage, F_{ND} is the fraction of the pore space that contains colloids that has not been drained, and f_r is the fraction of colloids that is released from drained portions of the SWI. The value of f_r is expected to be high when $d_c > w_f$ and the adhesive force is low. Conversely, f_r will be much lower in regions with $d_c < w_f$ or when the adhesive force is strong. It should be mentioned that S_i may vary spatially with depth, the water saturation history, and size of the pore space (enhanced retention has been observed in grain-grain contacts and large scale surface roughness locations). Initially, we assume that retained colloids are uniformly distributed on the SWI at a particular location, but may vary with depth. Equation (9) indicates that S is directly related to S_i and decreases with a decrease in F_{ND} (drainage to a lower water content).

Information about A_s and $A_{aw}(\theta)$ (equation (8)) can be used to determine F_{ND} as

$$F_{ND}(\theta) = \frac{A_s - A_{aw}(\theta)}{A_s - A_{aw}(\theta_i)}, \tag{10}$$

where θ_i [L^{3}L^{-3}] is the initial volumetric water content during colloid deposition. Note that $\theta < \theta_i$ and $A_{aw}(\theta) > A_{aw}(\theta_i)$ during drainage. Equation (10) provides a nonlinear description of F_{ND} that decreases from 1 to 0 as θ decreases. Alternatively, a simple linear approximation of F_{ND} can be obtained from θ as

$$F_{ND} \approx \frac{\theta}{\theta_i}. \tag{11}$$

An equilibrium expression for colloid release during drainage can be derived from equation (9) by taking the partial derivative of S with respect to time. When using the nonlinear description of F_{ND} given by equation (10) the value of E_{swa} is given as

$$E_{swa} = \rho_b f_r S_i \frac{\partial F_{ND}}{\partial t} H_o\left(-\frac{\partial \theta}{\partial t}\right) = \rho_b f_r \left(\frac{S_i}{A_s - A_{aw}(\theta_i)}\right) \frac{dA_{aw}}{d\theta} \frac{\partial \theta}{\partial t} H_o\left(-\frac{\partial \theta}{\partial t}\right). \tag{12}$$

The value of E_{swa} for a linear description of F_{ND} (equation (11)) is given as

Table 4. Summary of Model Parameters and Pearson's Correlation Coefficient for D21g Release Experiments (Phase 3)

Figure #	Equation	IS (mM)	Cycle	f_r	f_{awi}	R^{2a}
2	14	5	1	0	0	0.68
3	12	5	1	1.80	0.61	0.93
3	13	5	1	0.92	0.61	0.93
4a	13	5	1	0.78	0.62	0.85
	13	5	2	0.47	0.34	
	13	5	3	0.21	0.6	
	13	5	4	0.10	0.07	
4b	13	5	1	0.75	0.48	0.82
	13	5	2	0.75	0.48	
	13	5	3	0.75	0.48	

[a]A single value of R^2 was determined for all drainage and/or imbibition cycles.

$$E_{swa} = \frac{\rho_b f_r S_i}{\theta_i} \frac{\partial \theta}{\partial t} H_o \left(-\frac{\partial \theta}{\partial t} \right).$$ (13)

The Heaviside functions in equations (12) and (13) were used to turn release on during drainage. *Cheng and Saiers* [2009] and *Russell et al.* [2012] proposed an expression similar to equation (13) to describe colloid release from the SWI to the aqueous phase during drainage and/or imbibition. Conversely, E_{swa} was partitioned in this work between the aqueous phase and the AWI during drainage using f_{awi} in equations (4) and (6), respectively. Only the portion of E_{swa} that enters that aqueous phase can be transported during drainage. Values of f_r and f_{awi} were obtained by inverse optimization to the release data during Phase 3 (Table 4).

Colloid mobilization due to a destruction of the AWI is modeled during imbibition as

$$E_{ra} = -\Gamma \frac{dA_{aw}}{d\theta} \frac{\partial \theta}{\partial t} H_o \left(\frac{\partial \theta}{\partial t} \right).$$ (14)

If a constant concentration of colloids on the AWI is assumed, then changes in A_{aw} during imbibition produce release given by equation (14). Entrapped air was not considered in equation (14) because of the many additional complexities and model parameters in hysteretic systems.

Zhang et al. [2012] accounted for release from the AWI to the aqueous phase during imbibition using an expression that was proportional to $\frac{\partial \theta}{\partial t}$. However, these authors did not consider the fraction of E_{swa} that partition to the AWI during drainage (equations (12) and (13)), and can be released during subsequent imbibition using equation (14).

Note that colloid release with transients in water content was initiated in equations (12–14) by changes in A_{aw} or θ with time. The AWS contact line advances as A_{aw} increases and θ decreases during water drainage. Similarly, destruction of the AWI occurs as the AWS contact line advances from smaller to larger pore spaces during water imbibition. Hence, $\frac{\partial \theta}{\partial t}$ and $\frac{\partial A_{aw}}{\partial t}$ can be thought of as an approximation for the rate of change in the triple contact line. The amount of release depends on this rate, as well as the initial conditions (S_i in equations (12) and (13), and Γ in equation (14)) and the removal efficiency (f_r).

3.6. Solution of Governing Equations

The above equations were implemented into the HYDRUS-1D model [*Šimůnek et al.*, 2008]. Richards equation (equation (1)) was solved using time-dependent water flux and pressure head boundary conditions at the top and bottom boundaries, respectively, and an initial uniform water saturation. The advective dispersion equation (equation (2)) was solved using a time-dependent solute flux boundary condition at the top boundary, a zero dispersive flux at the bottom boundary, and an initial condition of no colloids. The HYDRUS-1D model includes a nonlinear least square fitting routine to determine model parameters by optimizing model output to experimental data.

4. Results and Discussion

4.1. Breakthrough Curves

Wang et al. [2014] presented and discussed saturated and unsaturated D21g BTC data under various saturation conditions. Table 3 provides fitted retention model parameters (Phases 1 and 2) and the R^2 value for
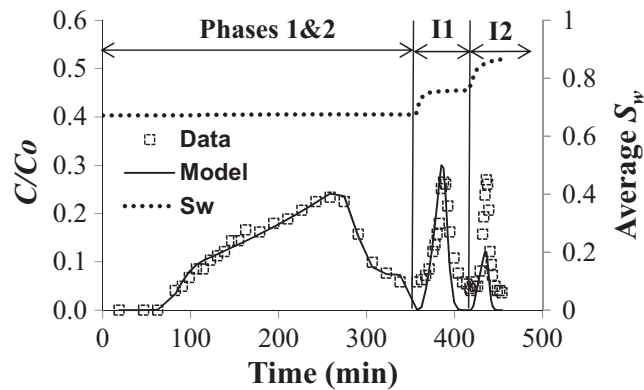
Figure 2. An example of observed [*Wang et al.*, 2014] and simulated D21g transport (Phases 1 and 2) and release (Phase 3) from the AWI during imbibition. Initial deposition occurred under unsaturated conditions (around 0.64 water saturation), and then the sand was saturated using two imbibition sequences (denoted by I1 and I2). See Tables (1–4) for experimental details and model parameters.

the goodness of model fit. The model description of the BTCs was very good ($R^2 > 0.92$). The value of S_i was determined at the end of the steady state, breakthrough curve simulation, and then used for simulations of D21g release during Phase 3 that will be discussed below.

4.2. Evaluation of E_{ra}

Figure 2 presents observed and simulated D21g transport under steady state, unsaturated flow when the water saturation was around 0.64 during Phases 1 and 2. This figure also shows the release behavior

when the sand was subsequently saturated using two imbibition sequences during Phase 3. The release model provided a reasonable description of the observed data for the first imbibition step even though no release model parameters were fitted during Phase 3 (Table 4). Note that the model predicts that only E_{ra} (equation (14)) contributed to cell release because $E_{swa} = 0$. Consequently, simulated release only occurred from the AWI and was initiated by destruction of the AWI during imbibition. The agreement between the simulation and experimental release provides a validation of equation (14) during the first imbibition step.

The release behavior for the second imbibition step was not described as well as the first imbibition step. The model predicts that all of the cells on the AWI will be released when the sand is completely saturated. The second predicted release pulse is smaller than the first because of a smaller change in A_{aw} (Figure 1). Deviation between the model prediction and experimental data in the second imbibition step occurs for several reasons. First, the experimental data never go to complete water saturation because of air entrapment. Our water flow simulation matches this experimental data, and therefore never reaches complete water saturation. Consequently, we also have incomplete removal from the AWI during imbibition in our simulation results. Second, equation (14) was derived under the assumption of a constant colloid concentration on the AWI. In reality, the colloid concentration on the AWI may increase during imbibition [*Keller and Auset*, 2007]. Equation (14) may therefore need to be modified to account for such second order processes by making Γ an increasing function of θ_w, but this was not attempted due to a lack of detailed experimental information.
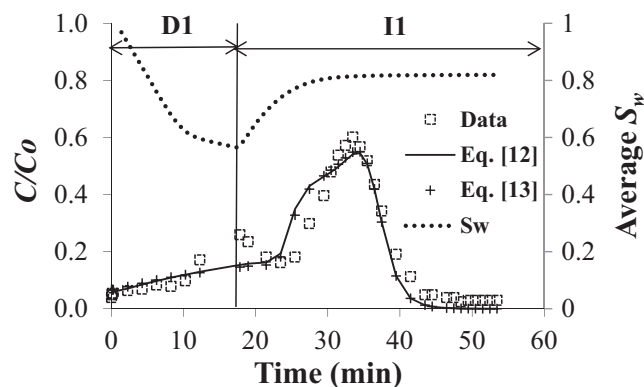

Figure 3. An example of observed [*Wang et al.*, 2014] and simulated D21g release during a drainage and imbibition cycle. Phases 1 and 2 were conducted under saturated conditions, and then the sand was drained and imbibed during Phase 3 by adjusting the boundary conditions at the bottom and top of the column. Simulation results are shown for models that employed equation (12) or equation (13). D# and I# denote the drainage and imbibition number (#), respectively. See Tables (1–4) for experimental details and model parameters.

4.3. Evaluation of E_{swa}

Figure 3 presents observed and simulated release (Phase 3) of D21g during a single drainage and imbibition cycle. In this case, Phases 1 and 2 were conducted under saturated conditions, and initial retention of the cells therefore only occurred on the SWI. Release from the SWI during Phase 3 was initiated by drainage when the bottom boundary condition was lowered to −90 cm and the water flux at the top was set to zero. Release was also induced during imbibition when the water flux was

changed from 0 to 24.3 mL min^{-1} at the column top. Two simulations are shown in the figure. One employed the nonlinear expression for F_{ND} to determine E_{swa} (equations (10) and (12)), whereas the other used the linear formulation for F_{ND} to quantify E_{swa} (equations (11) and (13)). Both models predict transfer of cells from the SWI to the aqueous phase and the AWI during drainage (E_{swa} in equations (12) and (13) is >0) because of a decrease in F_{ND}. Cells that partitioned from the SWI into the aqueous phase were transported with flowing water during drainage (equations (2), (4), (12), and (13)). Conversely, cells that partitioned from the SWI into the AWI were only released when the AWI was destroyed during imbibition (equations (7–14)). Transport of cells with the AWI was not considered in the model (equation (6)) because of the lack of experimental information to quantify this process and associated parameters.

The experimental release pulses of D21g were accurately simulated ($R^2 = 0.93$) using both models (equations (12) and (13)) when values of f_r and f_{awi} were fitted during Phase 3. The excellent agreement between the experimental data and simulations provides strong support for the conceptual model employed in equations (1–14). Recall that f_r accounts for the total amount of release from the SWI during drainage, whereas f_{awi} indicates the fraction of cells that partitioned to the AWI. The value of $f_{awi} = 0.61$ when using models based on equation (12) or equation (13) and this indicates that most of the released cells from the SWI partitioned to the AWI. Conversely, the value of f_r was higher when using equation (12) ($f_r = 1.8$) than equation (13) ($f_r = 0.92$). This high value of $f_r = 1.8$ reflects uncertainty in the initial estimate of A_s (equation (10)). In this case, equation (13) is preferred over equation (12) for simulating the transient release behavior because both models gave an equal description of the data ($R^2 = 0.93$), and equation (13) only requires information on readily accessible θ and θ_i values (rather than more difficult quantities of $A_{aw}(\theta)$, $A_{aw}(\theta_i)$, and A_s). We therefore employ equation (13) for the remaining simulations presented in this work.

Figure 4a presents observed and simulated D21g release (Phase 3) with repeated cycles of similar amounts of water drainage and imbibition (two steps). The peak effluent concentration in the release pulses decreased with increasing numbers of drainage and imbibition cycles. This trend reflects a decrease in the initial amount of cells on the SWI at the start of a drainage and imbibition cycle. However, the release model still did not provide an adequate description of the data when considering only a single value of f_r and f_{awi} (data not shown). Separate values of f_r and f_{awi} had to be fitted to each drainage and imbibition cycle in order to achieve good overall agreement between the data and model ($R^2 = 0.85$). Fitted values of f_r (from 0.78, to 0.47, to 0.21, and then to 0.10) and f_{awi} (from 0.62, to 0.34, to 0.06, and then to 0.07) rapidly decreased with increasing number of drainage and imbibition cycles. This decrease in cell release efficiency from the SWI and partitioning to the AWI likely reflects variations in cell accessibility and/or the strength of cell adhesion. All SWIs exhibit roughness to varying extents. Consequently, cells that are retained on an easily accessible region of the grain surface (e.g., a smooth surface) will be more readily removed by the AWI than cells in less accessible regions (e.g., the pits found on rough surfaces). Nanoscale roughness and/or chemical heterogeneity may also produce variability in the strength of cell adhesive [*Bradford and Torkzaban*, 2013]. Cells that exhibit a weaker adhesive force will be easily removed by the first drainage and imbibition cycle, whereas successive cycles will remove fewer cells because of their stronger adhesive force.

Figure 4b presents an example of observed and simulated D21g release during three continuous drainage and imbibition cycles when the column was successively drained to lower water saturations of 0.57, 0.36, and 0.27. The peak concentration and release amounts were observed to decrease for each drainage and imbibition cycle, but to a lesser extent than that shown in Figure 4a. In further contrast to Figure 4a, only a single value of $f_r = 0.75$ and $f_{awi} = 0.48$ needed to be fitted to the entire release data set to achieve good overall agreement between the data and model ($R^2 = 0.82$). These observations indicate that drainage to lower water saturations promoted greater amounts of cell release from the SWI, with relatively stable values of f_r and f_{awi} at different water saturations. This may be explained by an increased accessibility to S_i at lower water saturations (equations (9–14)) and a relatively constant water film thickness in drained portions of the pore space.

4.4. Numerical Experiments

Numerical experiments were conducted to better highlight the influence of f_r, f_{awi}, and initial and boundary conditions on cell release. Phases 1 and 2 were conducted under saturated conditions, and the initial retention of the cells therefore only occurred on the SWI. The same values of S_i with distance were employed in all simulations (determined using parameter values given in Table 3 for Figure 3). Release was initiated
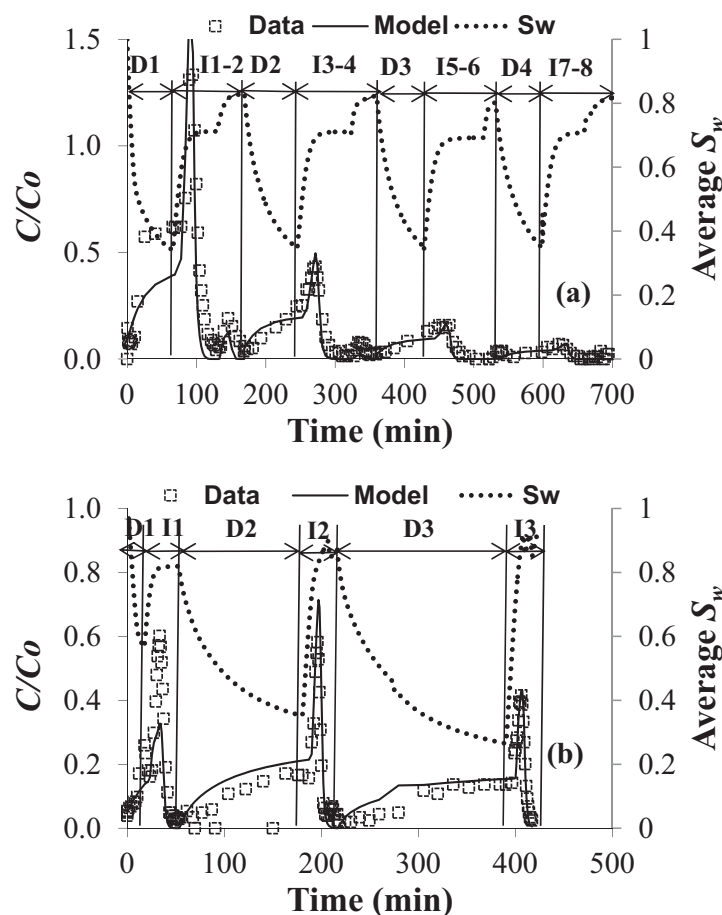
Figure 4. An example of observed [*Wang et al.*, 2014] and simulated D21g release with repeated cycles of water drainage and imbibition. Phases 1 and 2 were conducted under saturated conditions, and then the sand was repeatedly drained and imbibed during Phase 3 by adjusting the boundary conditions at the bottom and top of the column. In Figure 4a similar amounts of drainage and imbibition occurred with each cycle, whereas in Figure 4b the column was successively drained to lower water saturations of 0.57, 0.36, and 0.27. D# and I# denote the drainage and imbibition number (#), respectively. See Tables (1–4) for experimental details and model parameters.

during Phase 3 by a drainage and imbibition cycle. In this case, the bottom boundary condition was lowered to −90 cm and the water flux at the top was set to zero during drainage. Unless otherwise noted, the water flux was changed from 0 to 24.3 mL min^{-1} at the column top during imbibition.

Figure 5a presents simulations of D21g release during a single drainage and imbibition cycle when $f_{awi} = 0.5$ and values of f_r were varied (1, 0.75, 0.5, and 0.25). Equations (12) and (13) indicate that E_{swa} is proportional to f_r. The drainage and imbibition release curves and the total amount of release were therefore scaled with f_r. The value of f_r is expected to be strongly dependent on the strength of the adhesive interaction. Indeed, release pulses during drainage and imbibition have been shown to decrease with an increase in the solution ionic strength [*Cheng and Saiers*, 2009; *Zhuang et al.*, 2009; *Wang et al.*, 2014].

The value of E_{swa} is also proportional to S_i (equations (12) and (13)). Consequently, increasing values of S_i will scale the drainage and imbibition release curves in a similar manner to f_r in Figure 5a. This observation indicates that the amount of colloid release will be highly sensitive to the initial conditions. Greater values of S_i are expected with longer input pulse durations and concentrations, greater adhesive interactions (higher ionic strength), and lower hydrodynamic forces (lower water velocities) [*Bradford et al.*, 2009; *Sasidharan et al.*, 2014]. In addition, finer soil textures are commonly observed to produce greater values of S_i [*Liang et al.*, 2013]. *Wang et al.* [2014] observed that higher input pulse durations produced much greater amounts of D21g release during a drainage and imbibition cycle, and that these effects were more pronounced during imbibition.

Equation (14) indicates the amount of release from the AWI during imbibition (E_{ra}) is proportional to the initial value of Γ. Consequently, larger initial values of Γ are expected to produce greater amounts of release during subsequent imbibition events in a similar manner to Figure 5a. Under steady state unsaturated flow conditions the amount of colloid retention has been observed to increase with a decrease in θ_w [*Wan and Wilson*, 1994; *Schafer et al.*, 1998; *Gargiulo et al.*, 2008; *Torkzaban et al.*, 2008]. This increase in retention has been attributed to enhanced retention at the AWI and AWS triple line [*Schafer et al.*, 1998; *Auset et al.*, 2005; *Gao et al.*, 2006; *Chen et al.*, 2008; *Cheng and Saiers*, 2009]. It is therefore logical to anticipate greater amounts of colloid release will occur from the AWI when colloids are initially deposited at lower θ_w.
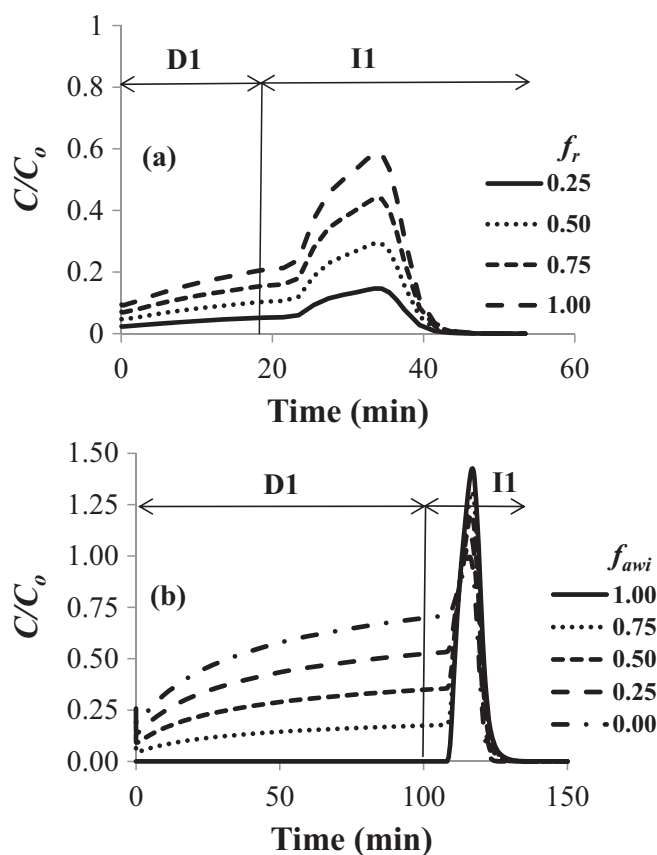
Figure 5. Simulated D21g release during a drainage and imbibition cycle for various values of f_r (f_{awi} = 0.5 in Figure 5a) and f_{awi} (f_r = 1 in Figure 5b). Phases 1 and 2 were conducted under saturated conditions, and then the sand was drained and imbibed during Phase 3 by adjusting the boundary conditions at the bottom and top of the column in a similar manner to Fig. 3. D# and I# denote the drainage and imbibition number (#), respectively.

Figure 5b presents simulations of D21g release during a single drainage and imbibition cycle when the drainage time was 100 min, f_r = 1 and values of f_{awi} were varied (0, 0.25, 0.5, 0.75, and 1). The value of f_{awi} had a dramatic influence on the drainage portion of the release curve, with increasing f_{awi} producing lower concentrations because less of the D21g mass partitioned into the aqueous phase. As expected (equation (14)), increases in f_{awi} caused an increase in D21g release during imbibition due to destruction of the AWI (peak relative concentrations ranged from 1 to 1.4). However, imbibition also yielded a cell release pulse even when f_{awi} = 0 due to an increase in the water flux that completed the drainage release pulse in the aqueous phase. Apparently, an increase in the water flux and destruction of the AWI produced similarly shaped release pulses during imbibition.

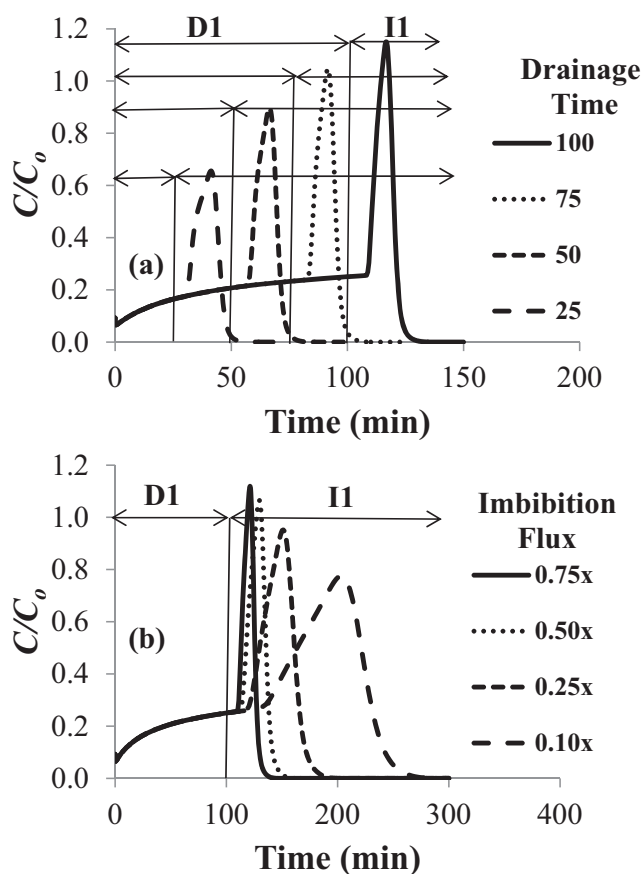It should be mentioned that the total mass of D21g released to the aqueous phase during the drainage and imbibition cycle was found to decrease with an increase in f_{awi} (Figure 5b). Higher values of f_{awi} partition more of the released cells from the SWI into the AWI. As mentioned previously (cf. Figure 2), not all of the cells were released from the AWI during imbibition because the optimized match between experimental and simulated water outflow (Table 1) did not allow for complete water saturation due to air entrapment. This information suggests that the AWI may act as a sink to retain cells that are released from the SWI. The above effects of f_{awi} on colloid release are expected to be more pronounced for hydrophobic and/or larger colloids that partition more readily to the AWI. The AWI and f_{awi} are also expected to play a more important role in finer textured soils because of their larger interfacial area [*Bradford and Leij*, 1997]. Additional research and model development is needed to fully resolve all of these issues.

Figure 6a presents simulations of D21g release during a single drainage and imbibition cycle when the duration of the drainage phase was varied (25, 50, 75, and 100 min). Similar to Figure 4b, increasing the duration of the drainage phase produced lower final water contents (average θ = 0.18, 0.15, 0.14, and 0.13). Greater amounts of D21g release occurred with increasing drainage time because more of the pore space was drained. However, the concentration of released cells only gradually increased during the drainage phase because the water flow rate rapidly decreased with decreasing θ. The enhancement of cell release with drainage time was mainly apparent during subsequent imbibition. In particular, increasing the drainage time produced a systematic increase in the concentration of released cells during subsequent imbibition. This observation indicates a strong sensitivity of release behavior to the drainage time and water content, and provides an explanation for differences in the relative importance of drainage and imbibition

Figure 6. Simulated D21g release during a drainage and imbibition cycle for various values of drainage time (25, 50, 75, and 100 min in Figure 6a) and imbibition fluxes (0.1, 0.25, 0.5, and 0.75 × 24.3 mL min^{-1} in Figure 6b). Phases 1 and 2 were conducted under saturated conditions, and then the sand was drained and imbibed during Phase 3 by adjusting the boundary conditions at the bottom and top of the column in a similar manner to Figure 3. D# and I# denote the drainage and imbibition number (#), respectively.

release pulses reported in the literature [*Saiers et al.*, 2003; *Chen and Flury*, 2005; *Cheng and Saiers*, 2009; *Zhuang et al.*, 2009; *Zhang et al.*, 2012].

Figure 6b presents simulations of D21g release during a single drainage and imbibition cycle when the water flux at the column inlet was decreased during the imbibition phase (0.75, 0.5, 0.25, and 0.1 × 24.3 mL min^{-1}). Note that the area under the breakthrough curves in Figure 6b does not correspond with the release mass, since the fluxes are different for each curve. Decreasing the water flux during the imbibition phase produced lower final water contents (average $\theta = 0.28$, 0.26, 0.23, and 0.19), but did not influence the release behavior during drainage. The peak cell release concentration increased with increasing water flux because more of the AWI was destroyed at higher θ and this produced greater amounts of cell release (equation (14)). This prediction is consistent with the experimental observations shown in Figure 2, as well as results reported in the literature [*Shang et al.*, 2008].

5. Summary and Conclusions

A novel mathematic model was developed to simulate colloid release during transients in water content which commonly occur in the vadose zone. The model predicts that a fraction of the retained colloids on the SWI (f_r) can partition to the AWI (f_{awi}) and aqueous phase ($1 − f_{awi}$) as θ decreases and A_{aw} increases during drainage. Colloid release from the AWI or AWS triple line to the mobile water phase occurred during imbibition as A_{aw} was destroyed. The colloid release pulse during drainage and imbibition tended to reflect the amount of retained colloids that were partitioned from the SWI into the aqueous phase and AWI, respectively.

This model was employed to describe the release of *E. coli* D21g under transient water content conditions [*Wang et al.*, 2014]. Simulations provided a reasonable description of experimental D21g release during drainage and imbibition, and this provides strong support for the implemented conceptual model. Simulation results indicated that the value of f_r and f_{awi} decreased with increasing numbers of drainage and imbibition cycles at a similar water content, because remaining cells were less accessible (pore geometry) to receding water films or they were more strongly held to the SWI (heterogeneity). However, repeated cycles of drainage and imbibition to successively lower water contents produced similar values of f_r and f_{awi} due to decreases in the water film thickness and increases in A_{aw} at lower water contents, and/or enhanced cell retention in smaller regions of the pore space.

Numerical experiments were conducted to investigate the influence of model parameters, initial conditions, and saturation dynamics on colloid release. Drainage and imbibition release curves were demonstrated to be proportional to f_r, and the initial amount of retention on the SWI and AWI. Variations in the value of f_{awi} were found to have a pronounced influence on both drainage and imbibition release pulses due to changes in the partitioning of cells from the SWI to the aqueous phase and the AWI. Higher values of f_{awi} produced lower amounts of total recovery in the aqueous phase because air entrapment led to incomplete removal from the AWI. An increase in the drainage time produced lower θ and enhanced colloid release, especially during imbibition, because more of the colloids on the SWI were transferred to the AWI and/or aqueous phase. Decreases in the imbibition flow rate produced lower values of θ and smaller peak concentrations in the imbibition release pulse because of lower flow rates and greater A_{aw}.

Additional research is warranted to study the effects of transients in water content on colloid release for various soil textures, colloid types and sizes, and colloid hydrophobicity. The model presented in this work is expected to be a powerful tool to help understand and quantify such release processes.

References

Adamczyk, Z., B. Siwek, M. Zembala, and P. Belouschek (1994), Kinetics of localized adsorption of colloid particles, *Adv. Colloid Interface Sci.*, *48*, 151–280.

Aramrak, S., M. Flury, and J. B. Harsh (2011), Detachment of deposited colloids by advancing and receding air-water interfaces, *Langmuir*, *27*, 9985–9993.

Aramrak, S., M. Flury, J. B. Harsh, R. L. Zollars, and H. P. Davis (2013), Does colloid shape affect detachment of colloids by a moving air–water interface?, *Langmuir*, *29*, 5770–5780.

Aramrak, S., M. Flury, J. B. Harsh, and R. L. Zollars (2014), Colloid mobilization and transport during capillary fringe fluctuations, *Environ. Sci. Technol.*, *48*, 7272–7279.

Auset, M., A. A. Keller, F. Brissaud, and V. Lazarova (2005), Intermittent filtration of bacteria and colloids in porous media, *Water Resour. Res.*, *41*, W09408, doi:10.1029/2004WR003611.

Bradford, S. A., and H. Kim (2010), Implications of cation exchange on clay release and colloid-facilitated transport in porous media, *J. Environ. Qual.*, *39*, 2040–2046.

Bradford, S. A., and F. J. Leij (1997), Estimating interfacial areas for multi-fluid soil systems, *J. Contam. Hydrol.*, *27*, 83–105.

Bradford, S. A., and S. Torkzaban (2013), Colloid interaction energies for physically and chemically heterogeneous porous media, *Langmuir*, *29*, 3668–3676.

Bradford, S. A., H. N. Kim, B. Z. Haznedaroglu, S. Torkzaban, and S. L. Walker (2009), Coupled factors influencing concentration dependent colloid transport and retention in saturated porous media, *Environ. Sci. Technol.*, *43*, 6996–7002.

Chatterjee, N., S. Lapin, and M. Flury (2012), Capillary forces between sediment particles and an air-water interface, *Environ. Sci. Technol.*, *46*, 4411–4418.

Chen, G., and M. Flury (2005), Retention of mineral colloids in unsaturated porous media as related to their surface properties, *Colloids Surf. A*, *256*, 207–216.

Chen, L., D. A. Sabatini, and T. C. Kibbey (2008), Role of the air–water interface in the retention of TiO_2 nanoparticles in porous media during primary drainage, *Environ. Sci. Technol.*, *42*, 1916–1921.

Cheng, T., and J. E. Saiers (2009), Mobilization and transport of in situ colloids during drainage and imbibition of partially saturated sediments, *Water Resour. Res.*, *45*, W08414, doi:10.1029/2008WR007494.

Cheng, T., and J. E. Saiers (2010), Colloid-facilitated transport of cesium in vadose-zone sediments: The importance of flow transients, *Environ. Sci. Technol.*, *44*, 7443–7449.

Cherrey, K. D., M. Flury, and J. B. Harsh (2003), Nitrate and colloid transport through coarse Hanford sediments under steady state, variably saturated flow, *Water Resour. Res.*, *39*(6), 1165, doi:10.1029/2002WR001944.

Engstrom, E., R. Thunvik, R. Kulabako, and B. Balfors (2015), Water transport, retention and survival of *Escherichia coli* in unsaturated porous media: A comprehensive review of processes, models and factors, *Crit. Rev. Environ. Sci. Technol.*, *45*, 1–100.

Gao, B., J. E. Saiers, and J. N. Ryan (2004), Deposition and mobilization of clay colloids in unsaturated porous media, *Water Resour. Res.*, *40*, W08602, doi:10.1029/2004WR003189.

Gao, B., J. E. Saiers, and J. Ryan (2006), Pore-scale mechanisms of colloid deposition and mobilization during steady and transient flow through unsaturated granular media, *Water Resour. Res.*, *42*, W01410, doi:10.1029/2005WR004233.

Gargiulo, G., S. A. Bradford, J. Šimůnek, P. Ustohal, H. Vereecken, and E. Klumpp (2008), Bacteria transport and deposition under unsaturated flow conditions: The role of water content and bacteria surface hydrophobicity, *Vadose Zone J.*, *7*, 406–419.

Gómez-Suárez, C., H. C. van der Mei, and H. J. Busscher (2001), Air bubble-induced detachment of polystyrene particles with different sizes from collector surfaces in a parallel plate flow chamber, *Colloids Surf. A*, *186*, 211–219.

Keller, A. A., and M. Auset (2007), A review of visualization techniques of biocolloid transport processes at the pore scale under saturated and unsaturated conditions, *Adv. Water Resour. 30*, 1392–1407.

Kim, M. K., S. B. Kim, and S. J. Park (2008), Bacteria transport in an unsaturated porous media: Incorporation of air–water interface area model into transport modelling, *Hydrol. Processes*, *22*, 2370–2376.

Lazouskaya, V., and Y. Jin (2008), Colloid retention at air–water interface in a capillary channel, *Colloids Surf. A, 325*, 141–151.

Lazouskaya, V., L.-P. Wang, H. Gao, X. Shi, K. Czymmek, and Y. Jin (2011), Pore-scale investigation of colloid retention and mobilization in the presence of a moving air–water interface, *Vadose Zone J.*, *10*, 1250–1260.

Lazouskaya, V., L.-P. Wang, D. Or, G. Wang, J. L. Caplan, and Y. Jin (2013), Colloid mobilization by fluid displacement fronts in channels, *J. Colloid Interface Sci.*, *406*, 44–50.

Leverett, M. C. (1941), Capillary behavior in porous solids, *Trans. Am. Inst. Min. Metall. Pet. Eng.*, *142*, 152–169.

Liang, Y., S. A. Bradford, J. Šimůnek, H. Vereecken, and E. Klumpp (2013), Sensitivity of the transport and retention of stabilized silver nanoparticles to physicochemical factors, *Water Res.*, *47*, 2572–2582.

Richards, L. A. (1931), Capillary conduction of liquids through porous media, *Physics*, *1*, 318–333.

Russell, T. L., K. M. Yamahara, and A. B. Boehm (2012), Mobilization and transport of naturally occurring enterococci in beach sands subject to transient infiltration of seawater, *Environ. Sci. Technol.*, *46*, 5988–5996.

Saiers, J. E., and J. J. Lenhart (2003), Colloid mobilization and transport within unsaturated porous media under transient-flow conditions, *Water Resour. Res.*, *39*(1), 1019, doi:10.1029/2002WR001370.

Saiers, J. E., G. M. Hornberger, D. B. Gower, and J. S. Herman (2003), The role of moving air-water interfaces in colloid mobilization within the vadose zone, *Geophys. Res. Lett.*, *30*(21), 2083, doi:10.1029/2003GL018418.

Sasidharan, S., S. Torkzaban, S. A. Bradford, P. J. Dillon, and P. G. Cook (2014), Coupled effects of hydrodynamic and solution chemistry on long-term nanoparticle transport and deposition in saturated porous media, *Colloids Surf. A*, *457*, 169–179.

Schafer, A., H. Harms, and A. J. B. Zehnder (1998), Bacterial accumulation at the air-water interface, *Environ. Sci. Technol.*, *32*, 3704–3712.

Shang, J., M. Flury, G. Chen, and J. Zhuang (2008), Impact of flow rate, water content, and capillary forces on in situ colloid mobilization during infiltration in unsaturated sediments, *Water Resour. Res.*, *44*, W06411, doi:10.1029/2007WR006516.

Shang, J., M. Flury, and Y. Deng (2009), Force measurements between particles and the air-water interface: Implications for particle mobilization in unsaturated porous media, *Water Resour. Res.*, *45*, W06420, doi:10.1029/2008WR007384.

Sharma, P., M. Flury, and J. Zhou (2008), Detachment of colloids from a solid surface by a moving air-water interface, *J. Colloid Interface Sci.*, *326*, 143–150.

Šimůnek, J., C. He, L. Pang, and S. A. Bradford (2006), Colloid-facilitated solute transport in variably saturated porous media, *Vadose Zone J.*, *5*, 1035–1047.

Šimůnek, J., M. Th. van Genuchten, and M. Šejna (2008), Development and applications of the HYDRUS and STANMOD software packages and related codes, *Vadose Zone J.*, *7*(2), 587–600, doi:10.2136/VZJ2007.0077.

Torkzaban, S., S. M. Hassanizadeh, J. F. Schijven, and A. M. de Roda Husman (2006a), Virus transport in saturated and unsaturated sand columns, *Vadose Zone J.*, *5*, 877–885.

Torkzaban, S., S. M. Hassanizadeh, J. F. Schijven, and H. H. J. L. van den Berg (2006b), Role of air–water interfaces on retention of viruses under unsaturated conditions, *Water Resour. Res.*, *42*, W12S14, doi:10.1029/2006WR004904.

Torkzaban, S., S. A. Bradford, M. Th. van Genuchten, and S. L. Walker (2008), Colloid transport in unsaturated porous media: The role of water content and ionic strength on particle straining, *J. Contam. Hydrol.*, *96*, 113–127.

van Genuchten, M. T. (1980), A closed-form equation for predicting the hydraulic conductivity of unsaturated soils, *Soil Sci. Soc. Am. J.*, *44*, 892–898.

Wan, J., and T. K. Tokunaga (1997), Film straining of colloids in unsaturated porous media: Conceptual model and experimental testing, *Environ. Sci. Technol.*, *31*, 2413–2420.

Wan, J., and J. L. Wilson (1994), Colloid transport in unsaturated porous media, *Water Resour. Res.*, *30*, 857–864.

Wang, Y., S. A. Bradford, and J. Šimůnek (2013), Transport and fate of microorganisms in soils with preferential flow under different solution chemistry conditions, *Water Resour. Res.*, *49*, 2424–2436, doi:10.1002/wrcr.20174.

Wang, Y., S. A. Bradford, and J. Šimůnek (2014), Release of *E. coli* D21g with transients in water content, *Environ. Sci. Technol.*, *48*, 9349–9357, doi:10.1021/es501956k.

Zevi, Y., B. Gao, W. Zhang, V. L. Morales, M. E. Cakmak, E. A. Medrano, W. Sang, and T. S. Steenhuis (2012), Colloid retention at the meniscus-wall contact line in an open microchannel, *Water Res.*, *46*, 295–306.

Zhang, Q. L., S. M. Hassanizadeh, A. Raoof, M. T. van Genuchten, and S. M. Roels (2012), Modeling virus transport and remobilization during partially saturated flow, *Vadose Zone J.*, *11*, doi:10.2136/vzj2011.0090.

Zhuang, J., J. F. McCarthy, J. S. Tyner, E. Perfect, and M. Flury (2007), In situ colloid mobilization in Hanford sediments under unsaturated transient flow conditions: Effect of irrigation pattern, *Environ. Sci. Technol.*, *41*, 3199–3204.

Zhuang, J., J. S. Tyner, and E. Perfect (2009), Colloid transport and remobilization in porous media during infiltration and drainage, *J. Hydrol.*, *377*, 112–119.